Article

Structure

Specific Interaction of the Human Mitochondrial Uncoupling Protein 1 with Free Long-Chain Fatty Acid

Graphical Abstract

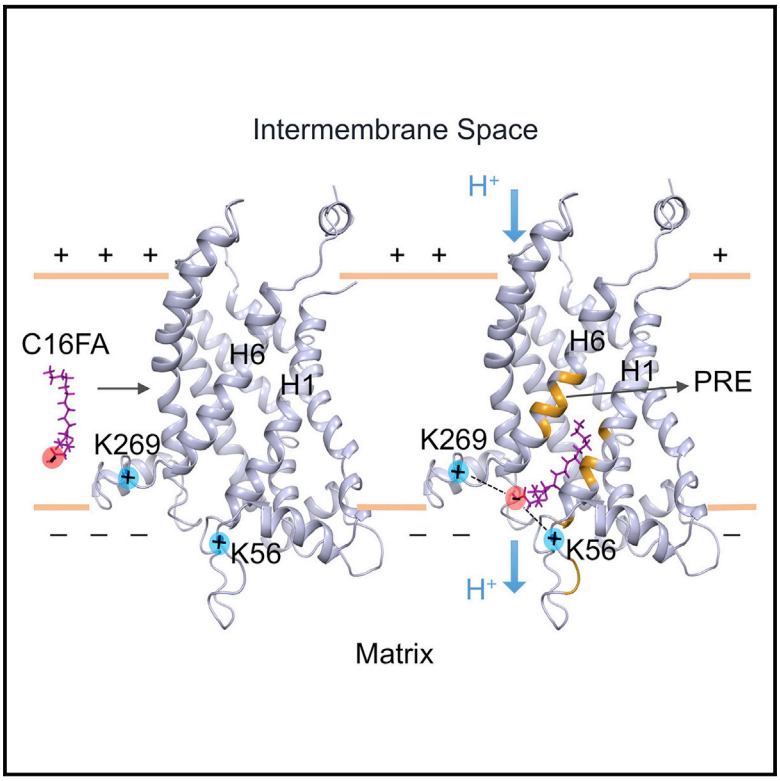

Authors

Linlin Zhao, Shuqing Wang, Qianli Zhu, Bin Wu, Zhijun Liu, Bo OuYang, James J. Chou

Correspondence

ouyang@sibcb.ac.cn (B.O.), james_chou@hms.harvard.edu (J.J.C.)

In Brief

The uncoupling protein UCP1 plays an essential role in thermogenesis of mammals; it generates heat by causing proton leak across the mitochondrial inner membrane that requires fatty acid. Zhao et al. report a specific fatty acid binding site of UCP1 that is functionally relevant to the proton transport activity of UCP1.

Highlights

- Developed high-resolution NMR system for human uncoupling protein 1 (UCP1)
- Achieved NMR resonance assignment for the 292-residue membrane protein
- Identified a specific fatty acid (FA) binding site in UCP1
- Showed that the FA binding site is required for UCP1-mediated H^+ transport

Zhao et al., 2017, Structure *25*, 1371–1379
September 5, 2017
http://dx.doi.org/10.1016/j.str.2017.07.005

Structure
Article

Specific Interaction of the Human Mitochondrial Uncoupling Protein 1 with Free Long-Chain Fatty Acid

Linlin Zhao,[1] Shuqing Wang,[2] Qianli Zhu,[1] Bin Wu,[1] Zhijun Liu,[1] Bo OuYang,[1,*] and James J. Chou[1,3,4,*]
[1]State Key Laboratory of Molecular Biology, National Center for Protein Science Shanghai, Shanghai Science Research Center, Shanghai Institute of Biochemistry and Cell Biology, Chinese Academy of Sciences, University of Chinese Academy of Sciences, Shanghai 201203, China
[2]School of Pharmacy, Tianjin Medical University, Tianjin 300070, China
[3]Department of Biological Chemistry and Molecular Pharmacology, Harvard Medical School, Boston, MA 02115, USA
[4]Lead Contact
*Correspondence: ouyang@sibcb.ac.cn (B.O.), james_chou@hms.harvard.edu (J.J.C.)
http://dx.doi.org/10.1016/j.str.2017.07.005

SUMMARY

The mitochondrial uncoupling protein 1 (UCP1) generates heat by causing proton leak across the mitochondrial inner membrane that requires fatty acid (FA). The mechanism by which UCP1 uses FA to conduct proton remains unsolved, and it is also unclear whether a direct physical interaction between UCP1 and FA exists. Here, we have shown using nuclear magnetic resonance that FA can directly bind UCP1 at a helix-helix interface site composed of residues from the transmembrane helices H1 and H6. According to the paramagnetic relaxation enhancement data and molecular dynamics simulation, the FA acyl chain appears to fit into the groove between H1 and H6 while the FA carboxylate group interacts with the basic residues near the matrix side of UCP1. Functional mutagenesis showed that mutating the observed FA binding site severely reduced UCP1-mediated proton flux. Our study identifies a functionally important FA-UCP1 interaction that is potentially useful for mechanistic understanding of UCP1-mediated thermogenesis.

INTRODUCTION

The mitochondrial uncoupling protein 1 (UCP1) found in the brown and beige adipocytes of mammals play the dominant role in adaptive thermogenesis (Almind et al., 2007; Cannon and Nedergaard, 2004; Klingenberg, 2010; Wu et al., 2012), although a recent study suggests that alternative UCP1-independent thermogenic factors also exist in these cells (Long et al., 2016). UCP1 is localized in the inner membrane of mitochondria; it translocates proton (H^+) down the H^+ concentration gradient, and generates heat by dissipating the energy contained in the H^+ electrochemical potential across the inner membrane, which otherwise can be used for ATP synthesis (reviewed in Klingenberg, 2010 and Krauss et al., 2005). This H^+ leak, or uncoupling of ATP synthesis from the oxidation of metabolites by UCP1, is activated by free fatty acids (FA) and can be inhibited by purine nucleotides such as guanosine diphosphate (GDP) (Locke et al., 1982; Strieleman et al., 1985; Winkler and Klingenberg, 1994).

The precise mechanism by which UCP1 mediates H^+ flux in an FA-dependent manner remains undefined, and two major competing models exist. The *protonophoretic* model, proposed by Garlid et al. in 1996, based on liposome-based H^+ flux data, contends that free long-chain FA can flip its protonated (or unionized) carboxylate head group across the inner membrane and release the H^+ to the matrix side driven by the pH gradient. The role of UCP1 is to then flip back the ionized FA, which cannot flip-flop on its own, to the intermembrane-space side for another H^+-carrying cycle. In this model, FA acts as a protonophore, and UCP1 does not directly transport H^+ but instead recycles the FA for sustained H^+ shuttling. Another model is the *H^+ shuttling* model, proposed more recently by Fedorenko et al. (2012) and based on patch-clamp data, in which UCP1 acts as an FA/H^+ symporter. This model requires the acyl chain terminus of FA to be strongly anchored to UCP1 such that the FA head group is inside the UCP1 cavity and can shuttle H^+ across the cavity. Although the two models are profoundly different, both require the ability of UCP1 to transport ionized FA across the membrane. This functionality of UCP1 has indeed been evidenced by liposome and patch-clamp assays that demonstrated UCP1-catalyzed transport of alkyl sulfonate, an ionized analog of FA (Fedorenko et al., 2012; Garlid et al., 1996).

In an earlier study we found that UCP2, another member of the UCP family, can specifically bind free long-chain FA with its peripheral site between H1 and H6 near the matrix side of the protein (Berardi and Chou, 2014). In the binding site, electrostatic interactions between the FA carboxylate and basic residues of the protein in and near the amphipathic helix h1 are important for both UCP2-mediated H^+ and FA transport (Berardi and Chou, 2014). Since FA binding to the UCP2 periphery is unlikely to rearrange the protein cavity to acquire H^+ conductance, the observed coupling between the FA binding site and H^+ flux in that study seem to be more consistent with the protonophoretic mechanism. We nevertheless emphasize that the above argument is indirect, as the only direct proof of the

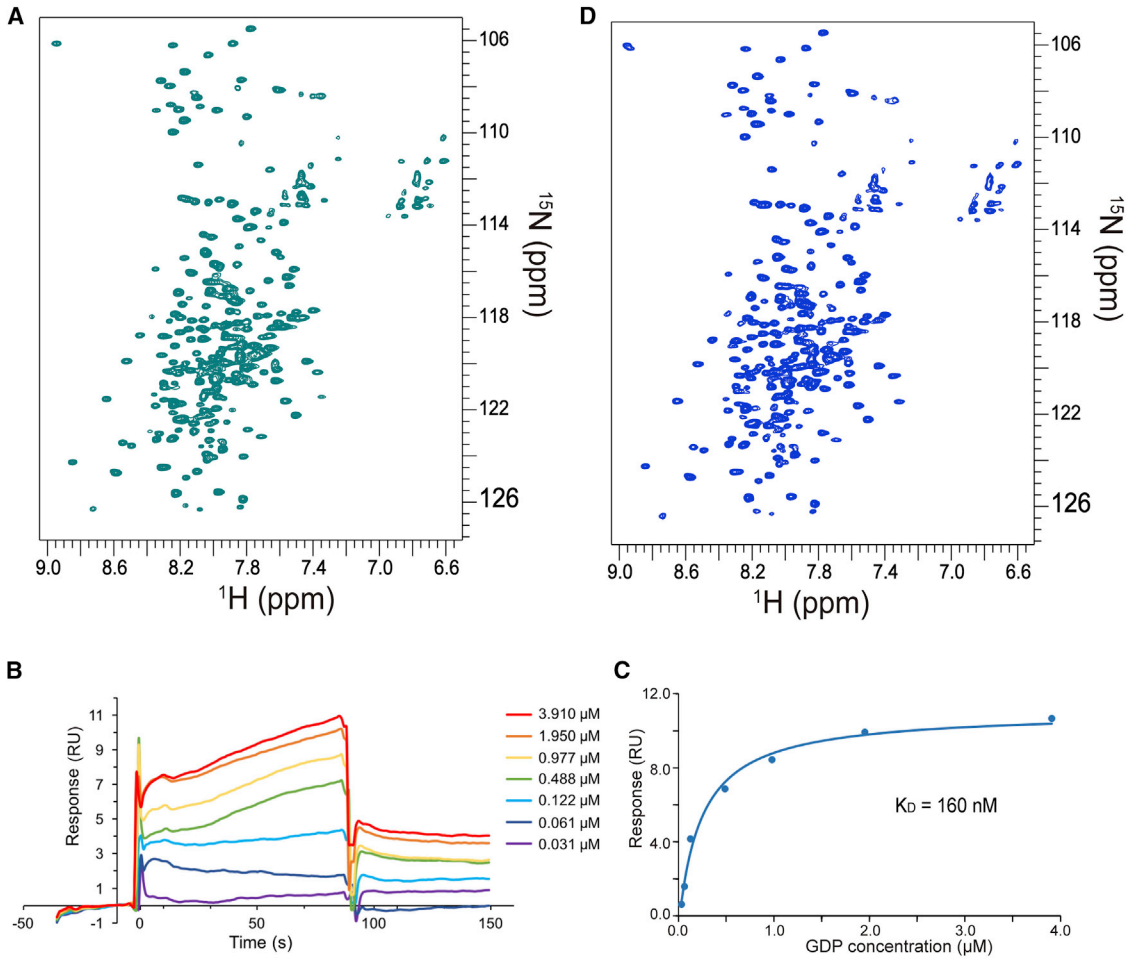

Figure 1. Specific GDP Binding of UCP1 Reconstituted in FC-12

(A) 2D ^{1}H-^{15}N TROSY-HSQC spectrum of 0.5 mM *U*-[^{15}N,^{13}C,^{2}H]UCP1 in the presence of 60 mM FC-12 recorded at 600 MHz (^{1}H frequency) and 30°C.

(B) SPR binding sensorgrams of GDP binding to UCP1 at various GDP concentrations in the presence of 3 mM FC-12. The GDP concentrations are 0.031 μM (purple), 0.061 μM (blue), 0.122 μM (cyan), 0.488 μM (green), 0.977 μM (yellow), 1.950 μM (orange), and 3.910 μM (red).

(C) Fitting data in (B) to the equilibrium binding equation yielded apparent K_D of 160 nM.

(D) 2D ^{1}H-^{15}N TROSY-HSQC spectrum of 30 μM *U*-[^{15}N,^{13}C,^{2}H]UCP1 in the presence of 3 mM FC-12 recorded as in (A).

protonophoretic model would be showing one UCP-mediated FA flip-flop per H^+ translocated across the membrane.

Although *in vitro* UCP2 showed functional similarities to UCP1, i.e., its H^+ translocation requires FA and can be inhibited by purine nucleotides such as GDP (Jaburek et al., 1999), the physiological function of UCP2 is not heat generation, and mounting evidence suggests that UCP2 does not have uncoupling activities *in vivo* (Nedergaard and Cannon, 2003; Stuart et al., 2001). In fact, a more recent study showed that UCP2 can catalyze the exchange of malate, oxaloacetate, and aspartate for phosphate and H^+, and that its physiological role may be to limit the oxidation of acetyl-coenzyme A-producing substrates such as glucose and to prevent the mitochondrial accumulation of C4 metabolites by exporting them out of mitochondria (Vozza et al., 2014). These newly reported transport activities of UCP2 are independent of FA. Therefore, based on the large differences in the physiological function, it is not immediately justified to extrapolate the mechanism of UCP2 to UCP1. Moreover, according to the 59% sequence identity between UCP1 and UCP2, it is also not obvious that the two structures should be the same.

This study aimed to address direct interaction between UCP1 and FA, which is recognized as a mandatory step in the activation of UCP1-mediated uncoupling activities (Fedorenko et al., 2012; Garlid et al., 1996). To tackle this problem, we first developed a UCP1 sample system that can generate high-resolution nuclear magnetic resonance (NMR) spectra and thus affords comprehensive chemical-shift analysis and secondary structure characterization. We then performed paramagnetic relaxation enhancement (PRE) measurements using FAs with different spin-label positions and found a specific FA binding site that is functionally important to UCP1-mediated H^+ flux.

RESULTS

An NMR-Feasible Sample of UCP1

Solution NMR is a versatile tool with which residue-specific ligand binding of a membrane protein can be identified using

Figure 2. Primary and Secondary Structure Alignment of Human UCP1 and Mouse UCP2

The cylinders above the sequence indicate the helical regions of the mouse UCP2 NMR structure (PDB: 2LCK). Asterisks below the sequence indicate the UCP1 residues with NMR chemical-shift assignment, and dots indicate helical regions of UCP1 predicted by TALOS+ based on chemical-shift values, i.e., TALOS+ output shows "GOOD" prediction with $\phi/\psi = -60°/-40° \pm 30°$. UCP2 residues previously shown to interact with FA are highlighted with red boxes (Berardi and Chou, 2014).

the simple titration or nuclear Overhauser enhancement (NOE) method, and this was demonstrated previously for several mitochondrial membrane proteins (Berardi and Chou, 2014; Jaremko et al., 2014; Run et al., 2015). This application is, however, only valid if a functionally relevant NMR sample can be developed for the membrane protein of interest, especially when detergent micelles could potentially cause protein misfolding. As in the case of UCP2 (Berardi et al., 2011), we developed an NMR sample of human UCP1 reconstituted in the Foscholine-12 (FC-12) micelles. The human UCP1 (residues 13–304 with a C-terminal 6× His tag) was expressed in *Escherichia coli* as inclusion bodies and extracted with FC-12 under denaturing conditions. The protein was purified by Ni-affinity chromatography and refolded by removing denaturant and excessive detergent. The refolded protein was separated from the misfolded protein aggregates using a series of Q and SP columns, and was further purified to homogeneity by size-exclusion chromatography (see STAR Methods).

The NMR sample of UCP1 in FC-12 generated a ^{1}H-^{15}N correlation spectrum of good resolution and dispersion (Figure 1A). However, titrating the NMR sample with GDP showed only small chemical-shift perturbation of the backbone amides even at very high GDP concentration (~1 mM), which seemed inconsistent with the tight GDP binding reported for UCP1 reconstituted in a more native environment (Lee et al., 2015). We speculated two plausible reasons. First, the FC-12 detergent caused significant disruption of the UCP1 structure such that GDP can no longer bind. Second, GDP binding in the cavity mostly involve contacts with side chains and thus can only induce small chemical-shift changes of the backbone amides. In fact, earlier NMR studies of carrier proteins never observed large chemical-shift perturbations by cavity-binding substrates (Run et al., 2015) except for the binding of the inhibitor CATR to the ADP/ATP carrier (Bruschweiler et al., 2015).

We then examined GDP binding of the UCP1 NMR sample using an independent biophysical method, surface plasma resonance (SPR). In this experiment, UCP1 in 3 mM FC-12 was immobilized onto the sensor chip, and GDP solutions with concentration ranging from 15.25 nM to 31.25 μM were the flow-through analytes. The SPR results clearly showed interaction between UCP1 and GDP in FC-12 with an estimated dissociation constant (K_D) of 160 nM (Figures 1B and 1C). The protein and detergent concentrations used in the SPR experiment were 30 μM and 3 mM, respectively, much lower than the NMR sample concentrations (0.5 mM UCP1 and 60 mM FC-12), which led us to further test whether detergent concentration has any denaturing effect on UCP1. We recorded a spectrum of a reconstituted UCP1 sample collected directly as elution from size-exclusion chromatography without concentration. This sample contains ~30 μM UCP1 and 3 mM FC-12 and generated a ^{1}H-^{15}N correlation spectrum (Figure 1D) essentially identical to that at higher protein and detergent concentration (Figure 1A). Based on these results, we can conclude that the human UCP1 reconstituted in FC-12 is folded, as indicated by the good NMR chemical-shift dispersion, and is capable of binding GDP according to the SPR data. The K_D of GDP binding in the NMR sample (160 nM) is still about 4-fold higher than that of UCP1 in more native environment (40 nM) (Lee et al., 2015). Some of the causes for the discrepancy in K_D could be the different detergents used for protein reconstitution and the absence of cardiolipin in the NMR sample that was reported to be important for stabilizing GDP binding of UCP1 (Lee et al., 2015). Despite the lower than expected GDP affinity, we believe the UCP1 in the NMR sample is qualitatively in a relevant state for gathering structural clues about FA binding.

Secondary Structure Mapping of UCP1 by NMR

We assigned ~75% of the backbone resonances of non-proline residues using a combination of triple-resonance and NOE experiments (Figure 2) (STAR Methods). The majority of the unassigned residues are in the regions T134–T155 and T194–L216, possibly due to exchange broadening. Two sets of chemical shifts were detected for residues L26–G45, indicating the presence of two different conformations (Figure S1A). It is unclear whether this observation was an artifact of proline

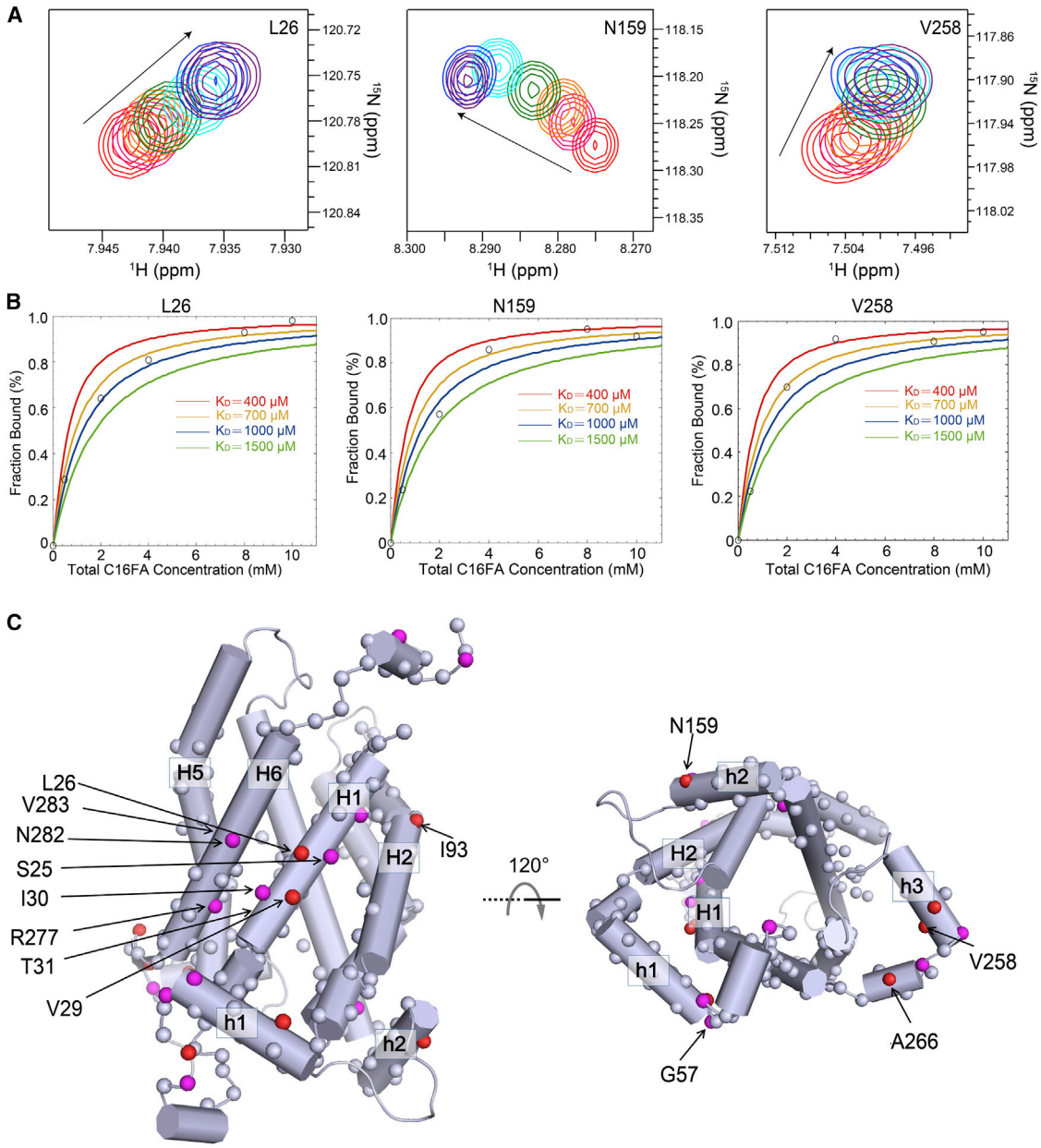

Figure 3. Characterization of C16FA Binding to UCP1 by Chemical-Shift Titration

(A) Examples of residue-specific chemical-shift perturbations at various C16FA concentrations: 0 mM (red), 0.5 mM (pink), 1 mM (orange), 2 mM (green), 4 mM (cyan), 8 mM (blue), and 10 mM (purple). The peaks are from 2D ^{1}H-^{15}N TROSY-HSQC spectra recorded at 600 MHz (^{1}H frequency) with a 0.5 mM *U*-[^{15}N,^{13}C,^{2}H] UCP1 sample.

(B) Simulated binding curves (Equation 2) at various K_D values used to match the titration data from (A).

(C) Mapping the residues with higher apparent C16FA affinities onto the UCP1 model. Spheres represent the analyzed residues. Spheres are colored such that red represents $K_D \leq 700$ μM, magenta represents 700 μM < K_D <1,200 μM, and white represents $K_D \geq 1{,}200$ μM.

isomerization at P33 or due to functionally meaningful conformational states in slow exchange. The backbone ^{13}Cα, ^{13}Cβ, and ^{13}C′ chemical shifts were used with the TALOS+ program (Shen et al., 2009) to derive backbone dihedral angles (Cα secondary shifts shown in Figure S1B). The results show that the helical regions of UCP1 are similar to those of UCP2 (Figure 2) despite dissimilarity in their NMR spectra (Berardi and Chou, 2014). The overall agreement in local structural segments between UCP1 and UCP2 suggests that the two homologous carriers are structurally similar.

Fatty Acid Binding to UCP1 from Chemical-Shift Titration

To investigate FA binding, we first titrated UCP1 with FA having 16 carbons (C16FA) and monitored C16FA-induced chemical-shift changes using the 2D TROSY-HSQC (transverse relaxation

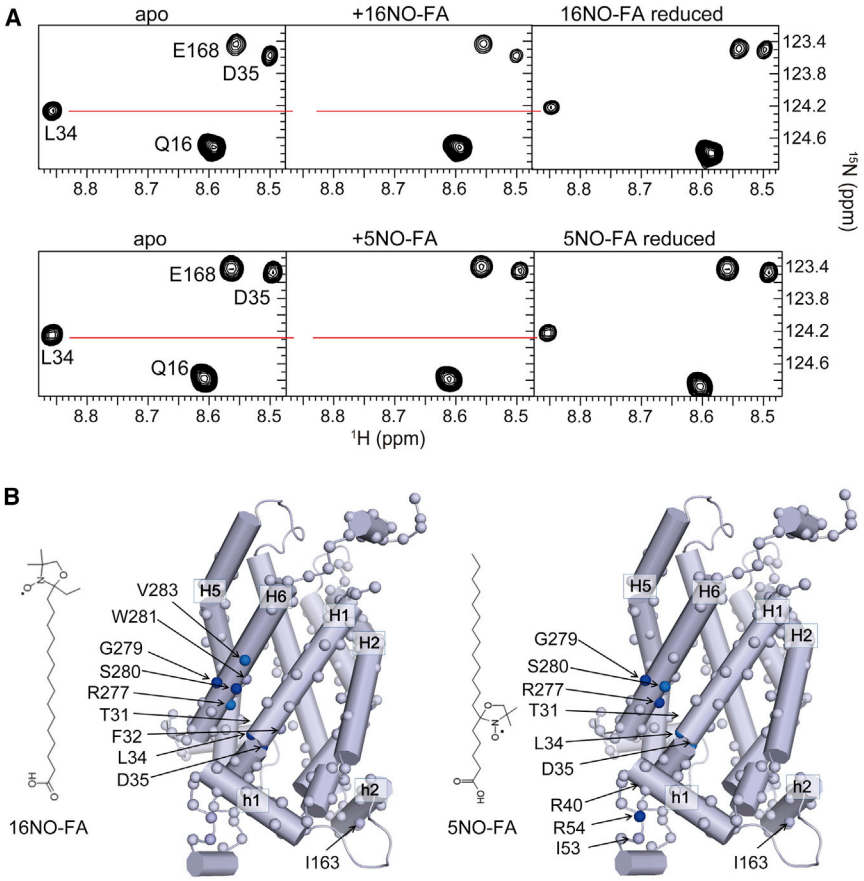

Figure 4. Unambiguous Identification of FA Binding to UCP1 Using Paramagnetic Probes

(A) Specific broadening of ^{1}H-^{15}N correlation peaks by different nitroxide-labeled FAs (16NO-FA and 5NO-FA) and recovery of the broadened peaks upon addition of ascorbic acid.

(B) Mapping the PREs induced by 16NO-FA (left) and 5NO-FA (right) onto the UCP1 model derived from the UCP2 NMR structure (PDB: 2LCK). Spheres represent analyzed residues. Blue spheres represent residues with $I/I_0 < 0.4$.

optimized spectroscopy and heteronuclear single-quantum coherence) experiment (Figure 3A). Residue-specific chemical-shift changes show a clear trend of binding saturation with K_D estimated to be 700 ± 200 μM (Figure 3B). We emphasize that due to strong partition of C16FA in detergent micelles, the effective concentration of FA is difficult to estimate, and thus the K_D values obtained only represent the apparent K_D in our NMR sample system. The non-linear chemical-shift changes (e.g., N159 and V258) suggest the presence of intermediate state(s) in addition to the unbound and FA-saturated states. To obtain a preliminary view of C16FA binding, we selected UCP1 residues in the top 20% in binding affinity (or low K_D) and mapped them onto the structural models of UCP1, which were constructed based on the NMR backbone structure of mouse UCP2 and the crystal structure of bovine AAC (ADP/ATP carrier), respectively, using Modeller9 (Webb and Sali, 2014). In both models, many residues in H1 and H6 showed obvious chemical-shift saturation and they include S25, L26, V29, I30, and T31 of H1 and R277, N282, and V283 of H6 (Figures 3C and S2). These residues appear to form a contiguous binding region for the FA. In addition, C16FA also caused some chemical-shift perturbation in other regions, e.g., I93 and N159 of H2 and h2, respectively.

The Fatty Acid Binding Site Determined Using the Spin-Labeled Fatty Acids

The C16FA partition in micelles could, in addition to direct interaction with UCP1, induce chemical-shift changes indirectly by altering the micelle properties. We thus used spin-labeled FAs to more directly probe the FA binding site by PRE. Two different spin-labeled C16FAs were used: one having the nitroxide moiety at the fifth methylene position (5NO-FA) and the other with the nitroxide placed at the 16th methylene position near the terminal methyl group (16NO-FA). The spin-labeled FAs were titrated separately into the UCP1 sample (Figures 4A and S3). For both 5NO-FA and 16NO-FA, residues with $I/I_0 < 0.4$ (Figure S4) are mapped onto the structural models. Unlike the broad chemical-shift changes in Figures 3C and S2, the PREs are more confined to H1 and H6. Both spin-labeled FAs induced strong PREs for R277, G279, and S280 of H6 and T31, L34, and D35 of H1 (Figures 4B and S5). Most of these residues are in the H1-H6 interface, indicating that the FA binds at the groove formed by these two transmembrane helices. There are, however, some differences in the PRE patterns generated by the two spin labels. The 5NO-FA also affected the region near the amphipathic helix h1 on the matrix side of the UCP1 (e.g., R54), whereas in the case of 16NO-FA, residues closer to the cytosol side of H6, such as V283, showed strong PRE (Figure 4B). Collectively, the PRE patterns from the two spin-labeled FAs indicate that C16FA binds at the H1-H6 interface near the matrix side of UCP1, and its orientation is such that the carboxylate head group and the acyl chain point to the matrix and cytosol sides of the protein, respectively.

Evaluation of the NMR-Derived C16FA Binding Site by Molecular Dynamics Simulation

The PRE results in Figures 4 and S5 suggest that a key driving force of FA binding is electrostatic interactions between the carboxylate head group of FA and several basic residues near the matrix sides of H1 and H6 of UCP1 (e.g., K56 and K269), similar to what was observed for UCP2 previously (Berardi and Chou, 2014). However, basic residues are also present at similar positions of the H2-H3 and H4-H5 interfaces, raising concerns about binding specificity. We thus investigated the stability of the observed C16FA binding by molecular dynamics (MD) simulation in the lipid bilayer environment. The simulation system consists of the UCP1 model and C16FA

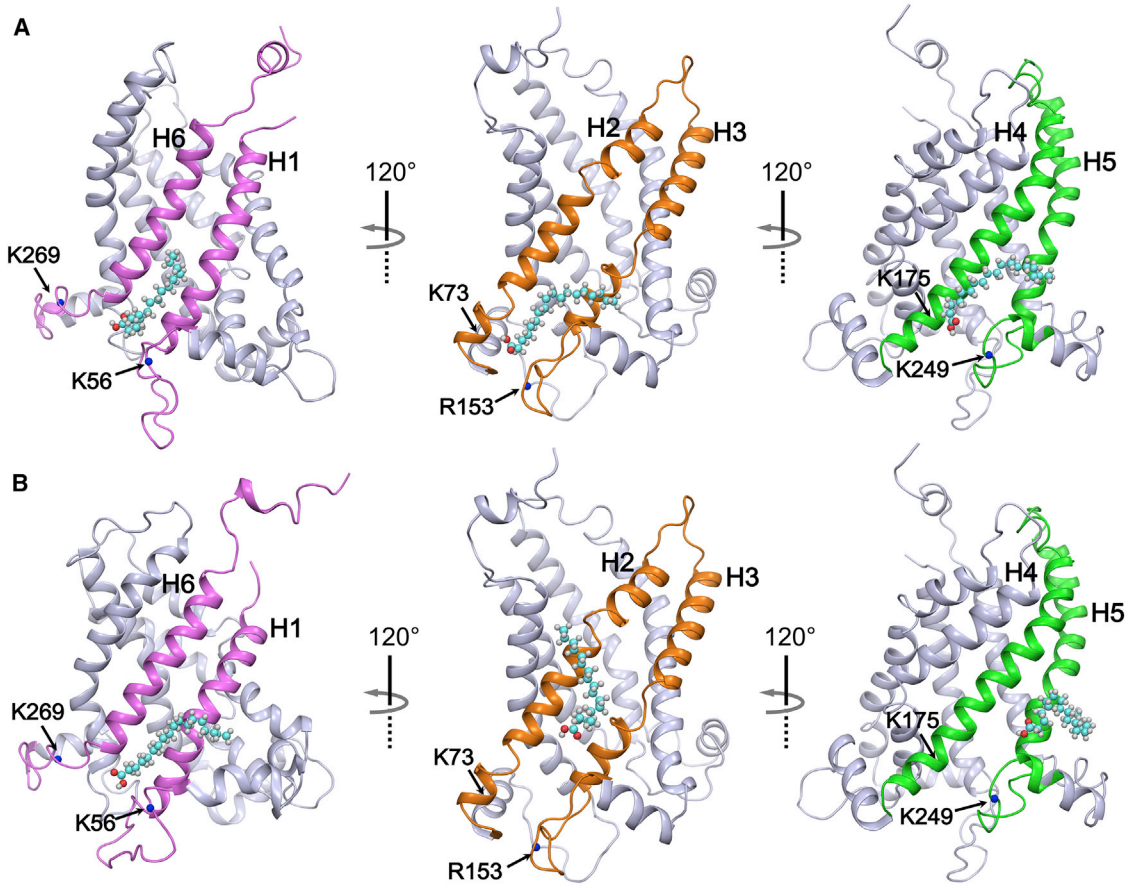

Figure 5. Stability of C16FA Binding to UCP1 Model in MD Simulation

(A) The initial positions of C16FAs at three helix-helix interface sites that afford charge-charge interactions with the FA carboxylate head group. These sites include the PRE-derived site at the H1-H6 interface (pink), the K73/R153 site at H2-H3 interface (orange), and the K175/K249 site at the H4-H5 interface (green).
(B) The average positions of C16FAs after 50 ns of MD simulation.

embedded in POPC (1-palmitoyl-2-oleoyl-*sn*-glycero-3-phosphocholine) lipid bilayer. Three C16FAs were initially positioned at three helix-helix interface sites that afford charge-charge interactions with the FA carboxylate head group. These sites include the PRE-derived site at the H1-H6 interface (residues K56 and K269), the K73/R153 site at H2-H3 interface, and the K175/K249 site at the H4-H5 interface (Figure 5A). Two MD stages were carried out for this system. The first stage was restrained MD whereby the protein backbone and the C16FA head group atoms were restricted with 100 kJ mol^{-1} $Å^{-2}$ whereas the protein side chains and C16FA acyl chains were allowed to move. Upon reaching equilibrium, the system was subject to the second stage, unrestrained simulation. After 50 ns of simulation, the C16FA in the H1-H6 site remained interacting with K56 and K269, whereas the other two C16FAs at the H2-H3 and H4-H5 sites diffused away from their corresponding basic residues (Figures 5B and S6). During the simulation, we also found that the acyl chain of the bound C16FA is flexible but overall is leaning toward H1. The simulation results suggest that the interaction between the FA carboxylate group and K56/K269 in the H1-H6 interface site of UCP1 is thermodynamically stable.

The NMR-Derived Fatty Acid Binding Site Is Critical for H^+ Conductance

Earlier site-directed mutagenesis of UCP1 has been focused mainly on the cavity-lining residues (Echtay et al., 2000; Jimenez-Jimenez et al., 2006; Urbankova et al., 2003). Here, we examined whether C16FA binding to the observed peripheral site is important for the H^+ conduction activity of UCP1 using a liposome-based H^+ flux assay. In this assay (Figure 6A), human UCP1 was reconstituted into liposomes made of a mixture of various lipids including DOPC (1,2-dioleoyl-*sn*-glycero-3-phosphocholine), DOPG (1,2-dioleoyl-*sn*-glycero-3-phospho-(10-rac-glycerol)), DOPE (1,2-dioleoyl-*sn*-glycero-3-phosphoethanolamine), and 14:0 CL (1,1′,2,2′-tetra-(9Z-octadecenoyl) cardiolipin). The protein/lipid ratio of 1:100 was used to make the proteoliposome. The K^+ concentrations inside and outside of the proteoliposomes were 5 and 100 mM, respectively. For measuring UCP1- and FA-mediated H^+ flux, the valinomycin was used to establish K^+ electrochemical potential to drive H^+ efflux, which was reported by the pH-sensitive fluorescent probe HPTS (8-hydroxypyrene-1,3,6-trisulfonic acid).

In the beginning of the assay, 80 μM C14FA was added to the proteoliposome solution. We first observed a clear trace of H^+

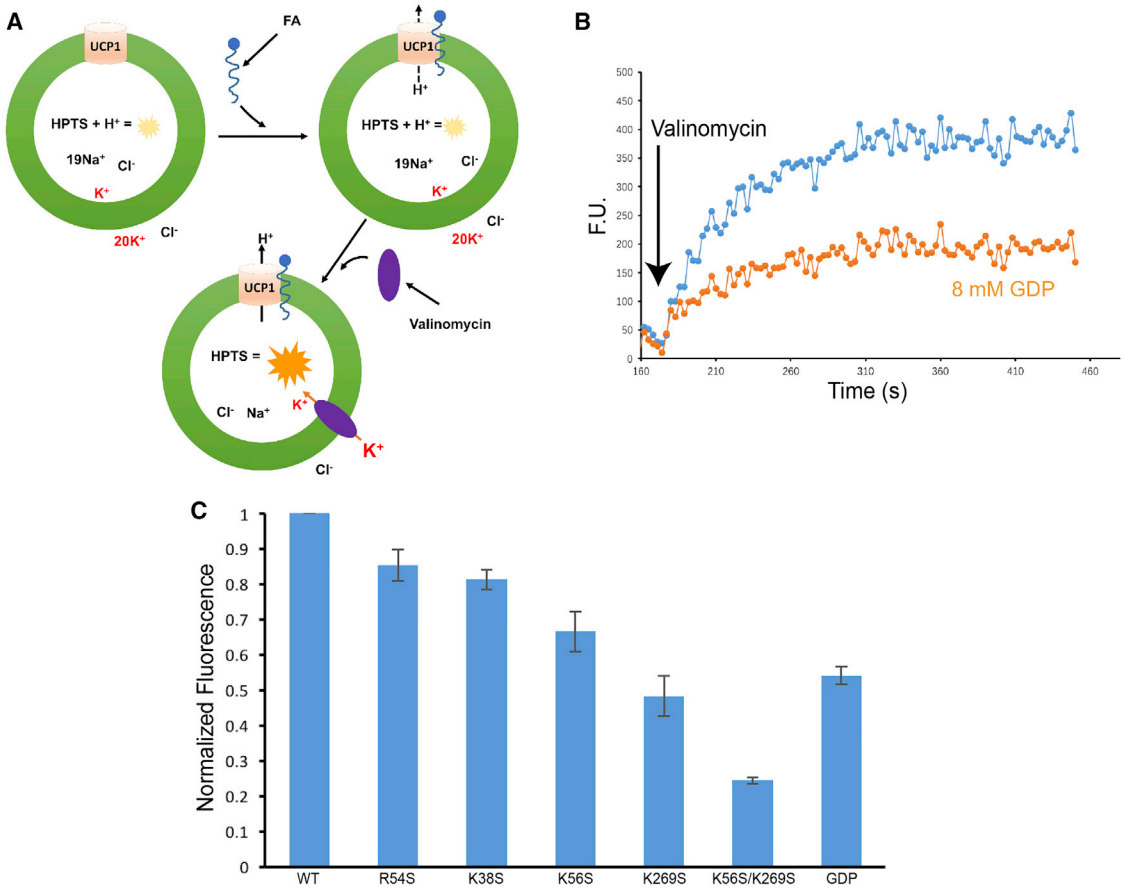

Figure 6. Effects of Mutating the FA Binding Site on UCP1-Mediated H^+ Flux

(A) Schematic illustration of the liposome assay for measuring UCP1-mediated H^+ flux. Valinomycin was used to generate K^+ electrochemical potential to drive H^+ efflux, leading to excitation of the pH-sensitive fluorescent probe HPTS.

(B) Time traces of fluorescence (F.U.) from the assay in (A) in the absence (blue) and presence (orange) of 8 mM GDP.

(C) Bar graph showing the ratios of H^+ flux of the mutants to that of the wild-type (WT). The error bars denote the SDs from three independent measurements.

flux upon adding 1.25 μM valinomycin to the system (Figure 6B). To examine whether the observed H^+ flux was specific for UCP1, we tested inhibition by GDP. At ~8 mM GDP, the H^+ flux was reduced by about 50% (Figure 6B), indicating that the H^+ flux was mostly mediated by UCP1. We then tested the effect of single mutations K56S and K269S as well as the double mutation K56S/K269S on UCP1-mediated H^+ flux. The results show that both single mutations decreased the flux rate by 50%–60% and the double mutation attenuated the rate by as much as 75% (Figure 6C). Notably, mutating K38 and R54, which are spatially close to K56, did not cause any significant decrease in H^+ flux (Figure 6C), suggesting that the observed FA binding to the H1-H6 interface site containing K56 is specific and essential for UCP1- and FA-mediated H^+ transport.

DISCUSSION

We have shown, using a combination of NMR titration and functional mutagenesis, that UCP1 has a functionally important FA binding site at the H1-H6 interface closer to the matrix side than the cytosol side of the protein. The importance of the basic residues, K56 of h1 and K269 at the matrix end of the H6, in FA- and UCP1-mediated H^+ flux suggest that FA binding is driven primarily by electrostatic interactions between the FA carboxylate head group and the positively charged lysines. The FA binding is specific for the following reason. In addition to K56 and K269, there are many positively charged residues both inside the carrier cavity and on the periphery that are accessible by FAs. These residues include K73 and R153 of the H2-H3 helix pair and K175 and K249 of the H4-H5 helix pair (Figure 5A). However, our titration experiments using spin-labeled C16FA only showed strong PRE for the site at the H1-H6 interface, indicating that electrostatic interaction is required but not sufficient for specific FA-UCP1 binding. Other factors such as the mode of FA partition around UCP1 as well as the relative positions of the basic and hydrophobic residues may also be important determinants of FA binding.

The FA binding of UCP1 is strikingly similar to that of UCP2 despite the two carriers having very different physiological functions. In UCP1, the hydrophobic groove at the H1-H6 interface is mostly formed by T31, F32, L34, D35, L278, G279, S280, W281, and V283. The similar hydrophobic groove between H1 and H6 was found in the FA binding site in UCP2. The electrostatic interaction of the FA carboxylate head group to K56 and K269 of UCP1 are important for UCP1 activity. The corresponding basic

residues in UCP2 (Figure 2), R60 and K271, have also been shown to be important for UCP2- and FA-mediated H^+ flux (Berardi and Chou, 2014). Both UCP1 and UCP2 have been demonstrated to mediate H^+ flux in an FA-dependent manner. Therefore, it is not surprising that the two carriers interact with FA in the similar manner. The common property of FA recognition between UCP1 and UCP2 further supports the notion that FA binding to the H1-H6 interface site represents an important step in FA- and UCP-mediated H^+ transport across the membrane.

Previous liposome-based and patch-clamp experiments have shown that both UCP1 and UCP2 are capable of flipping or transporting alkyl sulfonate (ASO^-), a mimetic of ionized FA, across the membrane, suggesting that these UCPs can catalyze FA flipping across their polar cavities (Berardi and Chou, 2014; Fedorenko et al., 2012). In fact, UCP1-mediated FA flipping across the membrane is mechanistically important as it is considered an essential step in both protonophoretic and proton-shuttling models (Fedorenko et al., 2012; Garlid et al., 1996; Klingenberg and Huang, 1999; Winkler and Klingenberg, 1994). In principle, FA binding to the H1-H6 interface is compatible with the FA flipping activity, as binding at this position potentially allows the insoluble FA to enter the polar cavity of UCP1 laterally from the membrane. We also note that the FA binding site reported here was observed in the NMR sample without any membrane potential. While this site is relevant for UCP1-mediated H^+ flux in our liposome assay, we cannot exclude the existence of other binding sites that are too lowly populated to be measured in the NMR sample but become stabilized under physiological condition by the strong potential of the mitochondrial inner membrane. For example, if the negatively charged carboxylate group of FA is inside the UCP1 cavity, the membrane potential could drive it to a binding site on the cytosol side of the protein.

STAR★METHODS

Detailed methods are provided in the online version of this paper and include the following:

- KEY RESOURCES TABLE
- CONTACT FOR REAGENT AND RESOURCE SHARING
- METHOD DETAILS
  - Sample Preparation
  - NMR Resonance Assignment
  - NMR Titration Experiments
  - SPR Analysis of UCP1-GDP Interaction
  - UCP1 Mediated H+ Flux Assay
  - Molecular Dynamics Simulation
- DATA AND SOFTWARE AVAILABILITY

SUPPLEMENTAL INFORMATION

Supplemental Information includes six figures and can be found with this article online at http://dx.doi.org/10.1016/j.str.2017.07.005.

AUTHOR CONTRIBUTIONS

L.Z., B.O., and J.J.C. conceived the study; L.Z. and Q.Z. prepared samples for structural and *in vitro* functional measurements; L.Z., B.W., and Z.L. collected NMR data; L.Z., B.O., and J.J.C. analyzed NMR data; L.Z. and Q.Z. performed liposome proton flux assays; S.W. performed MD simulations. J.J.C., L.Z., and B.O. wrote the paper; all authors contributed to editing of the manuscript.

ACKNOWLEDGMENTS

This work was supported by CAS grant XDB08030301 and National Natural Science Foundation of China grant 31570746 to J.J.C.

Received: April 21, 2017
Revised: June 16, 2017
Accepted: July 6, 2017
Published: August 3, 2017

REFERENCES

Almind, K., Manieri, M., Sivitz, W.I., Cinti, S., and Kahn, C.R. (2007). Ectopic brown adipose tissue in muscle provides a mechanism for differences in risk of metabolic syndrome in mice. Proc. Natl. Acad. Sci. USA *104*, 2366–2371.

Bartels, C., Xia, T.H., Billeter, M., Guntert, P., and Wuthrich, K. (1995). The program XEASY for computer-supported NMR spectral analysis of biological macromolecules. J. Biomol. NMR *6*, 1–10.

Berardi, M.J., and Chou, J.J. (2014). Fatty acid flippase activity of UCP2 is essential for its proton transport in mitochondria. Cell Metab. *20*, 541–552.

Berardi, M.J., Shih, W.M., Harrison, S.C., and Chou, J.J. (2011). Mitochondrial uncoupling protein 2 structure determined by NMR molecular fragment searching. Nature *476*, 109–113.

Bruschweiler, S., Yang, Q., Run, C., and Chou, J.J. (2015). Substrate-modulated ADP/ATP-transporter dynamics revealed by NMR relaxation dispersion. Nat. Struct. Mol. Biol. *22*, 636–641.

Cannon, B., and Nedergaard, J. (2004). Brown adipose tissue: function and physiological significance. Physiol. Rev. *84*, 277–359.

Delaglio, F., Grzesiek, S., Vuister, G.W., Zhu, G., Pfeifer, J., and Bax, A. (1995). NMRPipe: a multidimensional spectral processing system based on UNIX pipes. J. Biomol. NMR *6*, 277–293.

Deng, Z., Martyna, G.J., and Klein, M.L. (1992). Structure and dynamics of bipolarons in liquid ammonia. Phys. Rev. Lett. *68*, 2496–2499.

Echtay, K.S., Winkler, E., Bienengraeber, M., and Klingenberg, M. (2000). Site-directed mutagenesis identifies residues in uncoupling protein (UCP1) involved in three different functions. Biochemistry *39*, 3311–3317.

Fedorenko, A., Lishko, P.V., and Kirichok, Y. (2012). Mechanism of fatty-acid-dependent UCP1 uncoupling in brown fat mitochondria. Cell *151*, 400–413.

Garlid, K.D., Orosz, D.E., Modriansky, M., Vassanelli, S., and Jezek, P. (1996). On the mechanism of fatty acid-induced proton transport by mitochondrial uncoupling protein. J. Biol. Chem. *271*, 2615–2620.

Hoover, W.G. (1985). Canonical dynamics: equilibrium phase-space distributions. Phys. Rev. A *31*, 1695–1697.

Jaburek, M., Varecha, M., Gimeno, R.E., Dembski, M., Jezek, P., Zhang, M., Burn, P., Tartaglia, L.A., and Garlid, K.D. (1999). Transport function and regulation of mitochondrial uncoupling proteins 2 and 3. J. Biol. Chem. *274*, 26003–26007.

Jaremko, L., Jaremko, M., Giller, K., Becker, S., and Zweckstetter, M. (2014). Structure of the mitochondrial translocator protein in complex with a diagnostic ligand. Science *343*, 1363–1366.

Jimenez-Jimenez, J., Zardoya, R., Ledesma, A., Garcia de Lacoba, M., Zaragoza, P., Mar Gonzalez-Barroso, M., and Rial, E. (2006). Evolutionarily distinct residues in the uncoupling protein UCP1 are essential for its characteristic basal proton conductance. J. Mol. Biol. *359*, 1010–1022.

Jorgensen, W.L., and Tirado-Rives, J. (1988). The OPLS [optimized potentials for liquid simulations] potential functions for proteins, energy minimizations for crystals of cyclic peptides and crambin. J. Am. Chem. Soc. *110*, 1657–1666.

Kay, L.E., Torchia, D.A., and Bax, A. (1989). Backbone dynamics of proteins as studied by ^{15}N inverse detected heteronuclear NMR spectroscopy: application to staphylococcal nuclease. Biochemistry *28*, 8972–8979.

Klingenberg, M. (2010). Wanderings in bioenergetics and biomembranes. Biochim. Biophys. Acta *1797*, 579–594.

Klingenberg, M., and Huang, S.G. (1999). Structure and function of the uncoupling protein from brown adipose tissue. Biochim. Biophys. Acta *1415*, 271–296.

Krauss, S., Zhang, C.Y., and Lowell, B.B. (2005). The mitochondrial uncoupling-protein homologues. Nat. Rev. Mol. Cell Biol. *6*, 248–261.

Lee, Y., Willers, C., Kunji, E.R., and Crichton, P.G. (2015). Uncoupling protein 1 binds one nucleotide per monomer and is stabilized by tightly bound cardiolipin. Proc. Natl. Acad. Sci. USA *112*, 6973–6978.

Locke, R.M., Rial, E., Scott, I.D., and Nicholls, D.G. (1982). Fatty acids as acute regulators of the proton conductance of hamster brown-fat mitochondria. Eur. J. Biochem. *129*, 373–380.

Lomize, M.A., Lomize, A.L., Pogozheva, I.D., and Mosberg, H.I. (2006). OPM: orientations of proteins in membranes database. Bioinformatics *22*, 623–625.

Long, J.Z., Svensson, K.J., Bateman, L.A., Lin, H., Kamenecka, T., Lokurkar, I.A., Lou, J., Rao, R.R., Chang, M.R., Jedrychowski, M.P., et al. (2016). The secreted enzyme PM20D1 regulates lipidated amino acid uncouplers of mitochondria. Cell *166*, 424–435.

Nedergaard, J., and Cannon, B. (2003). The 'novel' 'uncoupling' proteins UCP2 and UCP3: what do they really do? Pros and cons for suggested functions. Exp. Physiol. *88*, 65–84.

Pervushin, K., Riek, R., Wider, G., and Wuthrich, K. (1997). Attenuated T2 relaxation by mutual cancellation of dipole-dipole coupling and chemical shift anisotropy indicates an avenue to NMR structures of very large biological macromolecules in solution. Proc. Natl. Acad. Sci. USA *94*, 12366–12371.

Run, C., Yang, Q., Liu, Z., OuYang, B., and Chou, J.J. (2015). Molecular basis of MgATP selectivity of the mitochondrial SCaMC carrier. Structure *23*, 1394–1403.

Schumann, F.H., Riepl, H., Maurer, T., Gronwald, W., Neidig, K.P., and Kalbitzer, H.R. (2007). Combined chemical shift changes and amino acid specific chemical shift mapping of protein-protein interactions. J. Biomol. NMR *39*, 275–289.

Shen, Y., Delaglio, F., Cornilescu, G., and Bax, A. (2009). TALOS+: a hybrid method for predicting protein backbone torsion angles from NMR chemical shifts. J. Biomol. NMR *44*, 213–223.

Strieleman, P.J., Schalinske, K.L., and Shrago, E. (1985). Fatty acid activation of the reconstituted brown adipose tissue mitochondria uncoupling protein. J. Biol. Chem. *260*, 13402–13405.

Stuart, J.A., Harper, J.A., Brindle, K.M., Jekabsons, M.B., and Brand, M.D. (2001). Physiological levels of mammalian uncoupling protein 2 do not uncouple yeast mitochondria. J. Biol. Chem. *276*, 18633–18639.

Urbankova, E., Hanak, P., Skobisova, E., Ruzicka, M., and Jezek, P. (2003). Substitutional mutations in the uncoupling protein-specific sequences of mitochondrial uncoupling protein UCP1 lead to the reduction of fatty acid-induced H^+ uniport. Int. J. Biochem. Cell Biol. *35*, 212–220.

Vozza, A., Parisi, G., De Leonardis, F., Lasorsa, F.M., Castegna, A., Amorese, D., Marmo, R., Calcagnile, V.M., Palmieri, L., Ricquier, D., et al. (2014). UCP2 transports C4 metabolites out of mitochondria, regulating glucose and glutamine oxidation. Proc. Natl. Acad. Sci. USA *111*, 960–965.

Vranken, W.F., Boucher, W., Stevens, T.J., Fogh, R.H., Pajon, A., Llinas, M., Ulrich, E.L., Markley, J.L., Ionides, J., and Laue, E.D. (2005). The CCPN data model for NMR spectroscopy: development of a software pipeline. Proteins *59*, 687–696.

Webb, B., and Sali, A. (2014). Comparative protein structure modeling using MODELLER. Curr. Protoc. Bioinformatics *47*, 5.6.1–5.6.32.

Winkler, E., and Klingenberg, M. (1994). Effect of fatty acids on H^+ transport activity of the reconstituted uncoupling protein. J. Biol. Chem. *269*, 2508–2515.

Wu, J., Bostrom, P., Sparks, L.M., Ye, L., Choi, J.H., Giang, A.H., Khandekar, M., Virtanen, K.A., Nuutila, P., Schaart, G., et al. (2012). Beige adipocytes are a distinct type of thermogenic fat cell in mouse and human. Cell *150*, 366–376.

Zhang, H., Sun, Y., Gao, S., Zhang, H., Zhang, J., Bai, Y., and Song, D. (2014). Studies of gold nanorod-iron oxide nanohybrids for immunoassay based on SPR biosensor. Talanta *125*, 29–35.

STAR★METHODS

KEY RESOURCES TABLE

REAGENT or RESOURCE	SOURCE	IDENTIFIER
Bacterial and Virus Strains		
pET-21a	Novagen	CB6490717
BL21 (DE3)	ThermoFisher	Cat#C600003
Chemicals, Peptides, and Recombinant Proteins		
Saturated hexadecanoic acid (C16FA)	Sigma-Aldrich	P5585; CAS: 57-10-3
Saturated tetradecanoic acid (C14FA)	Sigma-Aldrich	M3128; CAS: 544-63-8
5-DOXYL-stearic acid (5NO-FA)	Sigma-Aldrich	253634; CAS: 29545-48-0
16-DOXYL-stearic acid (16NO-FA)	Sigma-Aldrich	253596; CAS: 53034-38-1
1,2-dioleoyl-sn-glycero-3-phosphocholine (DOPC)	Avanti	850375P; CAS: 4235-95-4
1,2-dioleoyl-sn-glycero-3-phospho-(10-rac-glycerol) (DOPG)	Avanti	840475P; CAS: 67254-28-8
1,2-dioleoyl-sn-glycero-3-phosphoethanolamine (DOPE)	Avanti	850725P; CAS: 4004-05-1
1,1',2,2'-tetra-(9Z-octadecenoyl) cardiolipin (CL)	Avanti	750332P; CAS: 63988-21-6
8-hydroxypyrene-1,3,6-trisulfonic acid (HPTS)	Sigma-Aldrich	H1529; CAS: 6358-69-6 4004-05-1
Valinomycin	Sigma-Aldrich	R427187; MDL number: MFCD00066672
Critical Commercial Assays		
QuickChange II Site-Directed Mutagenesis Kit	Agilent Technologies	Cat #200523
Software and Algorithms		
Topspin	Bruker Corporation	https://www.bruker.com/products/mr/nmr/nmr-software/software/topspin
NMRPipe	Delaglio et al., 1995	https://spin-niddk-nih-gov.ezp-prod1.hul.harvard.edu/NMRPipe/
XEASY	Bartels et al., 1995	N/A
CcpNmr	Vranken et al., 2005	http://www.ccpn.ac.uk/v2-software/software
TALOS+	Shen et al., 2009	https://spin.niddk.nih.gov/bax/software/TALOS/
Modeller9	Webb and Sali, 2014	https://salilab.org/modeller/
Desmond 4.5	Schrödinger	https://www.schrodinger.com/desmond
BIAevaluation software 3.0	GE Healthcare	https://www.biacore.com/lifesciences/service/downloads/software_licenses/biaevaluation/
Pymol	The PyMOL Molecular Graphics System, Version 1.8 Schrödinger, LLC.	https://www.pymol.org
Softmax Pro 6.2.2	Molecular Devices	https://www.moleculardevices.com
Other		
Superdex-200 10/300GL column	GE Healthcare	17-5175-01
Ni-NTA resin	GE Healthcare	17-0575-02
HiTrap™ Q HP column	GE Healthcare	17-1153-01
HiTrap™ SP FF column	GE Healthcare	17-5054-01
CM5 sensor chip	GE Healthcare	BR100531
Biacore Amine Coupling Kit	GE Healthcare	BR100633

CONTACT FOR REAGENT AND RESOURCE SHARING

Further information and requests for resources and reagents should be directed to and will be fulfilled by the Lead Contact, James J. Chou (james_chou@hms.harvard.edu).

METHOD DETAILS

Sample Preparation

Human UCP1 gene (residues 13-304 with a C-terminal 6×His tag) was inserted into pET-21a vector and transformed into *E.coli* BL21. Protein expression was induced at cell culture OD_{600} ~0.7 with 0.5 mM IPTG for 3 hrs at 37°C. Cells were harvested and resuspended in *Resuspension Buffer* (50 mM Tris-HCl/pH 8.0, 200 mM NaCl). The cells were homogenized twice using high pressure homogenizer (AVESTIN: EmusiFlxe-C3) and centrifuged at 40,000 × g for 30 mins to collect inclusion body pellets. Inclusion bodies were dissolved in *Denaturing Buffer* (30 mM FC-12, 3 M guanidine, 150 mM NaCl, 20 mM HEPES/pH 7.5) overnight. Cell debris were removed by centrifugation at 40,000 × g for 30 mins. The denatured UCP1 (from 2 L cell culture) was loaded to a 10 mL Ni-NTA column and washed with 3 column volumes (CVs) of *Refolding Buffer* (6 mM FC-12, 150 mM NaCl, 20 mM HEPES/pH 7.5) 3 times, each time with increasing amounts of imidazole, 15, 20, and 30 mM, respectively. The protein was eluted with 5 CVs of *Elution Buffer* (250 mM imidazole, 6 mM FC-12, 150 mM NaCl, 20 mM HEPES/pH 7.5). The sample was then passed through Q HP and SP HP columns to remove aggregated and unfolded proteins. The flow-through was concentrated and further purified by size exclusion in the Superdex-200 10/300GL GE column in *FPLC Buffer* (20mM MES/pH 6.5, 30 mM NaCl, 3 mM FC-12). The size exclusion elution profile suggests that UCP1 is a homogeneous monomer. A typical UCP1 NMR sample contains 0.5 mM UCP1 in *NMR Buffer* (20 mM MES/pH 6.5, 30 mM NaCl, 60 mM FC-12). The UCP1 mutants (K56S, K269S, K56S/K269S, K38S, R54S) were expressed, purified, and refolded using the same protocol.

NMR Resonance Assignment

Sequence-specific assignment of backbone $^{1}H^{N}$, ^{15}N, $^{13}C^{\alpha}$, $^{13}C\beta$ and $^{13}C'$ resonances was accomplished using 3D TROSY-based HNCA, HN(CO)CA, HNCACB, HN(CO)CACB, HN(CA)CO and HNCO experiments (Kay et al., 1989; Pervushin et al., 1997). Additionally, the assignments were validated using a 3D (H^{N}, H^{N})-HSQC-NOESY-TROSY spectrum with ^{15}N, ^{15}N and $^{1}H^{N}$ evolution in the t_1, t_2 and t_3 dimensions, respectively, recorded with NOE mixing time of 250 ms. These experiments were performed using a 0.8 mM *U*-[^{15}N, ^{13}C, ^{2}H] UCP1 sample at 30°C on a 600 MHz Bruker spectrometer equipped with a cryogenic TXI probe. The NMR spectra were processed using NMRPipe (Delaglio et al., 1995) and analysed using XEASY (Bartels et al., 1995) and CcpNmr (Vranken et al., 2005).

NMR Titration Experiments

All NMR titration experiments were performed at 30°C on a 600 MHz Bruker spectrometer equipped with a cryogenic TXI probe. A 500 μl sample containing 0.5 mM *U*-[^{15}N, ^{13}C, ^{2}H] UCP1 in the above NMR buffer was titrated with 0, 2.5, 5, 10, 20, 40 and 50 μl C16FA stock solution (100 mM C16FA in 60 mM FC-12, 30 mM NaCl, 20 mM MES/pH 6.5), resulting in 0, 0.5, 1, 2, 4, 8, and 10 mM C16FA concentration points, respectively. At each C16FA concentration, a 2D TROSY-HSQC spectrum was acquired to follow C16FA induced chemical-shift perturbation. The combined chemical-shift differences ($\Delta\delta^{i}_{comb}$) were calculated for each residue using the formula (Schumann et al., 2007):

$$\Delta\delta^{i}_{comb} = \sqrt{\left(\omega_H \Delta\delta^{i}_{H}\right)^2 + \left(\omega_N \Delta\delta^{i}_{N}\right)^2}, \quad \text{(Equation 1)}$$

where $\Delta\delta^{i}_{H}$ and $\Delta\delta^{i}_{N}$ are ^{1}H and ^{15}N chemical-shift perturbations, respectively, and $\omega_H = 1.00$ and $\omega_N = 0.15$ are normalization factors. Apparent K_D was determined by fitting the data to the general solution of one-site binding:

$$\frac{[PS]}{[P_T]} = \frac{([P_T] + [S_T] + K_D) \pm \sqrt{([P_T] + [S_T] + K_D)^2 - 4[P_T][S_T]}}{2[P_T]}, \quad \text{(Equation 2)}$$

where $[P_T]$ is the total concentration of UCP1, $[S_T]$ is the total concentration of C16FA, and $[PS]$ is the concentration of the protein-ligand complex.

The same UCP1 sample as above was used for measuring PRE induced by the two paramagnetic NOFAs (16-DOXYL-stearic acid and 5-DOXYL-stearic acid, Sigma). The NOFA stock solutions were 2.5 mM NOFA in 30 mM FC-12, 30 mM NaCl, and 20 mM MES/pH 6.5. The stock solutions were added to two separate 500 μL / 0.5 mM UCP1 samples with the final NOFA concentrations of 0.25 and 0.5 mM for 16NOFA and 5NOFA, respectively. In both cases, 3D TROSY HNCO spectra were recorded before and after the addition of NOFAs. Residue-specific peak heights without (I_0) and with (I) NOFA were determined using the CcpNmr software. Residues with I/I_0 ratio < 0.4 were mapped onto the UCP1 structural model.

SPR Analysis of UCP1-GDP Interaction

Surface Plasma Resonance (SPR) experiments were performed with a Biacore T200 instrument (GE Healthcare) with CM5 sensor chip (GE Healthcare). Activation, deactivation and preparation of the coupled flow cell as well as the ligand-binding assay were performed essentially as described previously (Zhang et al., 2014). Briefly, the UCP1 in 3 mM FC-12 was immobilized in parallel-flow channels of CM5 sensor chip using Biacore Amine Coupling Kit (GE Healthcare). To investigate GDP-binding of UCP1, GDP solutions (3 mM FC-12, 25 mM MES/pH 6.5) with a series of GDP concentrations ranging from 15.25 nM to 31.25 μM were injected into the flow system. During the experiment, the analyte was injected at the flow rate of 25 μL/min and the running buffer consisted of 25 mM

MES/pH 6.5 and 3 mM FC-12. The association and dissociation times were 90 and 60 s, respectively. The binding constants were calculated using the 1:1 Langmuir binding model in the *BIAevaluation* software.

UCP1 Mediated H+ Flux Assay

The UCP1 proteoliposomes were made using a lipid composition of DOPC:DOPG:DOPE:CL (Avanti) at 20:5:1:1 molar ratio. A lipid solution containing 20 mg/mL lipids dissolved with 10% detergent (1:1 ratio of DM:OG) was prepared using *Buffer A* (10 mM MES/pH 6.0, 95 mM NaCl, and 5 mM KCl). A 0.5 mM UCP1 sample in the NMR buffer was mixed with the lipid solution at 100:1 lipid:protein ratio and then diluted 5x to a lipid concentration of 4 mg/mL with Buffer A in the presence of 60 μM pH-sensitive fluorescent probe HPTS (8-Hydroxypyrene-1,3,6-Trisulfonic Acid, Sigma). Detergent removal was performed twice using a G25 desalting column equilibrated with Buffer A. The resulting proteoliposomes contained the fluorescent probe and were stable at room temperature. The proteoliposome solution was further diluted 5x with *Buffer B* (10 mM MES/pH 6.0, and 100 mM KCl).

For measuring H^+ flux, 80 μM C14FA was first added to the external solution using a FA stock solution (40 mM C14FA dissolved in ethanol). Then 1.25 μM valinomycin (Sigma) was added to the external solution using the valinomycin stock solution (1.25 mM valinomycin in ethanol) to establish K^+ electrochemical potential to drive H^+ efflux. At the beginning of the experiment, pHs inside and outside of the proteoliposomes were equal. UCP1-mediated H^+ efflux resulted in internal pH increase, observed as a function of the HPTS florescence intensity at 510 nm (λ ex 460 nm) using SpectraMax M5 fluorometer (Molecular Devices) and Softmax Pro 6.2.2 software package. For measuring GDP inhibition, 8 mM GDP was added to the system.

Molecular Dynamics Simulation

Molecular dynamics (MD) simulations were performed using the academic free Desmond 4.5 package. OPLS-AA 2005 force field (Jorgensen and Tirado-Rives, 1988) in a neutral POPC (1-palmitoyl-2-oleoyl-sn-glycero-3-phosphocholine) bilayer with appropriate number of counter ions to balance the net charge of the system solvated in 0.15 M NaCl. The UCP1 model, derived using Modeller9 (Webb and Sali, 2014) from the UCP2 NMR structure (PDB code: 2LCK), was placed in the lipid bilayer according to its position defined in the Orientations of Proteins in Membranes (OPM) database (Lomize et al., 2006). The UCP1 model and three FAs in POPC bilayer were embedded in a periodic orthorhombic box ($\sim$14 × 14 × 14 $Å^3$) containing the explicit simple point charge (SPC) water molecules.

MD simulations were carried out with periodic boundary conditions in NPT ensemble in which the amount of substance (N), pressure (P) and temperature (T) were conserved. Nose-Hoover temperature coupling (Hoover, 1985) was used to calculate long-range electrostatic interactions with grid spacing of 0.8 Å. The RESPA integrator (Deng et al., 1992) was used for reducing calculation time by decreasing the frequency of time-consuming long-range interaction calculations. The real-space part electrostatic and van der Waals interactions were cut off at 9 Å.

The simulation consisted of two MD stages. The first stage was a restrained MD simulation performed using the default 'membrane relax' protocol provided in Desmond, in which the protein backbone and the C16FA head group atoms were restricted with 100 kJ mol^{-1} $Å^{-2}$ whereas the protein side chains and C16FA acyl chains were allowed to move. Upon reaching equilibrium, the system was subject to the second stage, the unrestrained MD, which was performed by running 50 ns of NPT production simulation without any restriction. The configurations and interval energy were recorded every 2 ps.

DATA AND SOFTWARE AVAILABILITY

NMR data were recorded using Topspin software from Bruker Biospin, and NMR data were processed using NMRPipe. NMR pulse sequences were mentioned and cited. Copies of the modified pulse sequences are available from the Lead Contact. Data were analyzed using XEASY for peak picking and resonance assignment. Analysis of peak intensities for titration experiments was performed using CcpNmr. Secondary structure prediction based on secondary chemical shift was performed using TALOS+. Protein homology model was built using Modeller9. Molecular dynamics simulations were performed using Desmond 4.5 package. Visualization and generation of molecular structure figures and images were created using PyMOL. All software resources are listed in the Key Resources Table, and the use of each package in the data analysis is described in the sub-headings of the STAR Methods.

Structure, Volume *25*

Supplemental Information

Specific Interaction of the Human Mitochondrial Uncoupling Protein 1 with Free Long-Chain Fatty Acid

Linlin Zhao, Shuqing Wang, Qianli Zhu, Bin Wu, Zhijun Liu, Bo OuYang, and James J. Chou

Supplemental Information

Specific Interaction of the Human Mitochondrial Uncoupling Protein 1 with Free Long-Chain Fatty Acid

Linlin Zhao[1], Shuqing Wang[2], Qianli Zhu[1], Bin Wu[1], Zhijun Liu[1], Bo OuYang[1]*,

James J. Chou[1,3]*

Supplemental Figures

Figure S1 Chemical shift assignment of UCP1. *Related to Figure 2, to show the presence of two different conformations in H1, and to show the helical regions of UCP1 as indicated by the Cα secondary shifts.*

Figure S2. Mapping the residues with higher apparent C16FA affinities onto the UCP1 model based on AAC crystal structure (PDB code: 1OKC). *Related to Figure 3C, to show the binding region of the fatty acid in AAC-based model is consistent with that in UCP2-based model.*

Figure S3. G279 shows specific broadening by nitroxide-labeled FAs and the recovery of broadened peaks by the addition of ascorbic acid. *Related to Figure 4, to show the broadening region of H6 as a supplementary for H1 in Figure 4A.*

Figure S4. Residue-specific FA-induced PRE. *Related to Figure 4, to provide a complete view of FA-induced PRE in UCP1.*

Figure S5. Mapping of the PRE effects under 16NO-FA and 5NO-FA onto the UCP1 model based on AAC crystal structure (PDB code: 1OKC). *Related to Figure 4, to show the broadening regions caused by NO-FAs in AAC-based model are consistent with that in UCP2-based model in Figure 4B.*

Figure S6. The MD simulation. *Related to Figure 5, to show the monitored distances between the UCP1 backbone amide nitrogen atoms of residues indicated by blue balls in Fig. 5B and the carbon atoms of the carboxyl groups of C16FA, and to show that the specific binding sites in H1-H6 in AAC-based model are consistent with that in UCP2-based model in Figure 5B.*

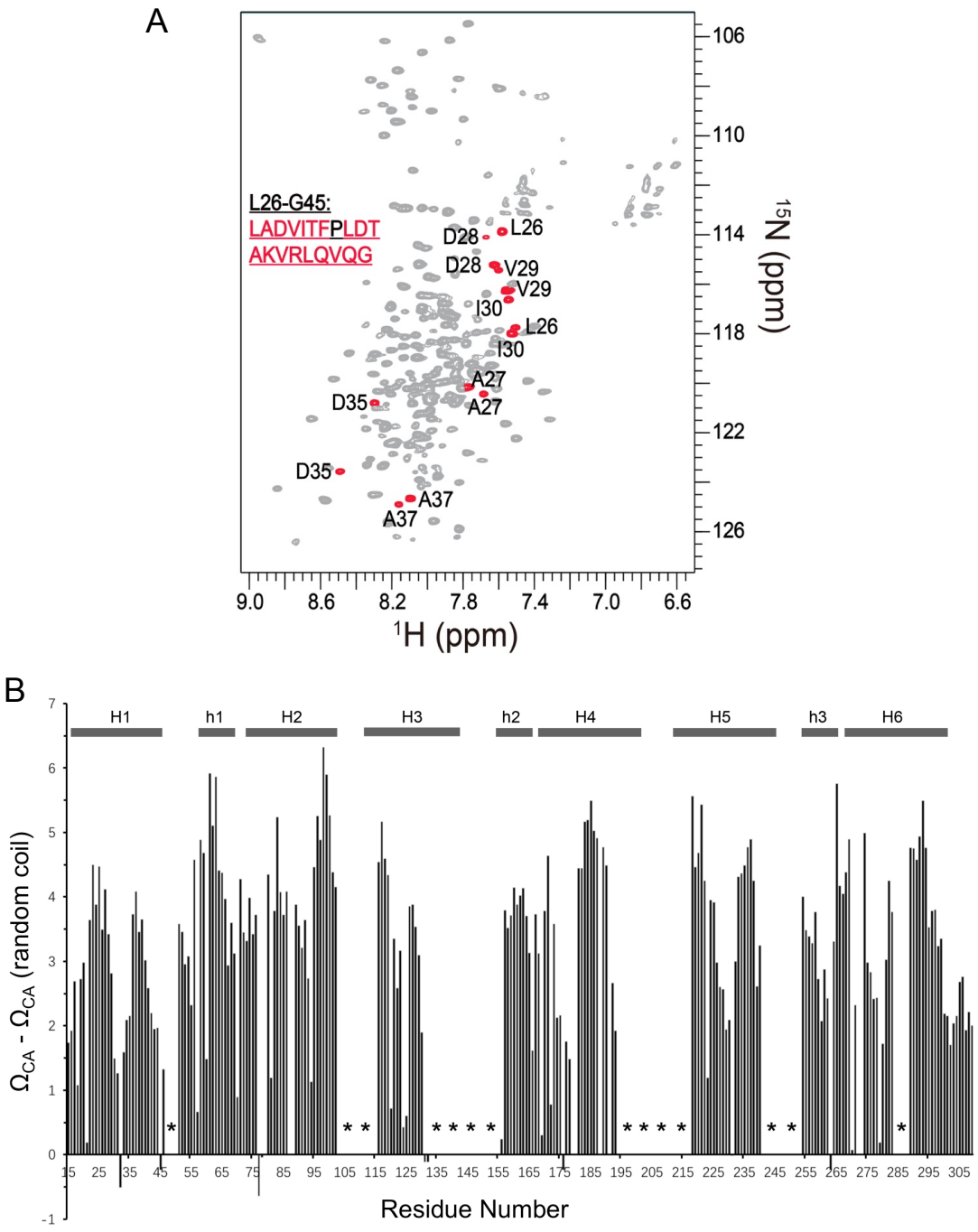

Figure S1. Chemical shift assignment of UCP1, Related to Figure 2.

(A) Examples for two pairs of backbone assignments from L26-G45. Those distinct residues in this region are colored by red.

(B) Residue-specific secondary chemical shift of Cα for showing the helical regions of UCP1. The '*' mark the regions with missing assignment.

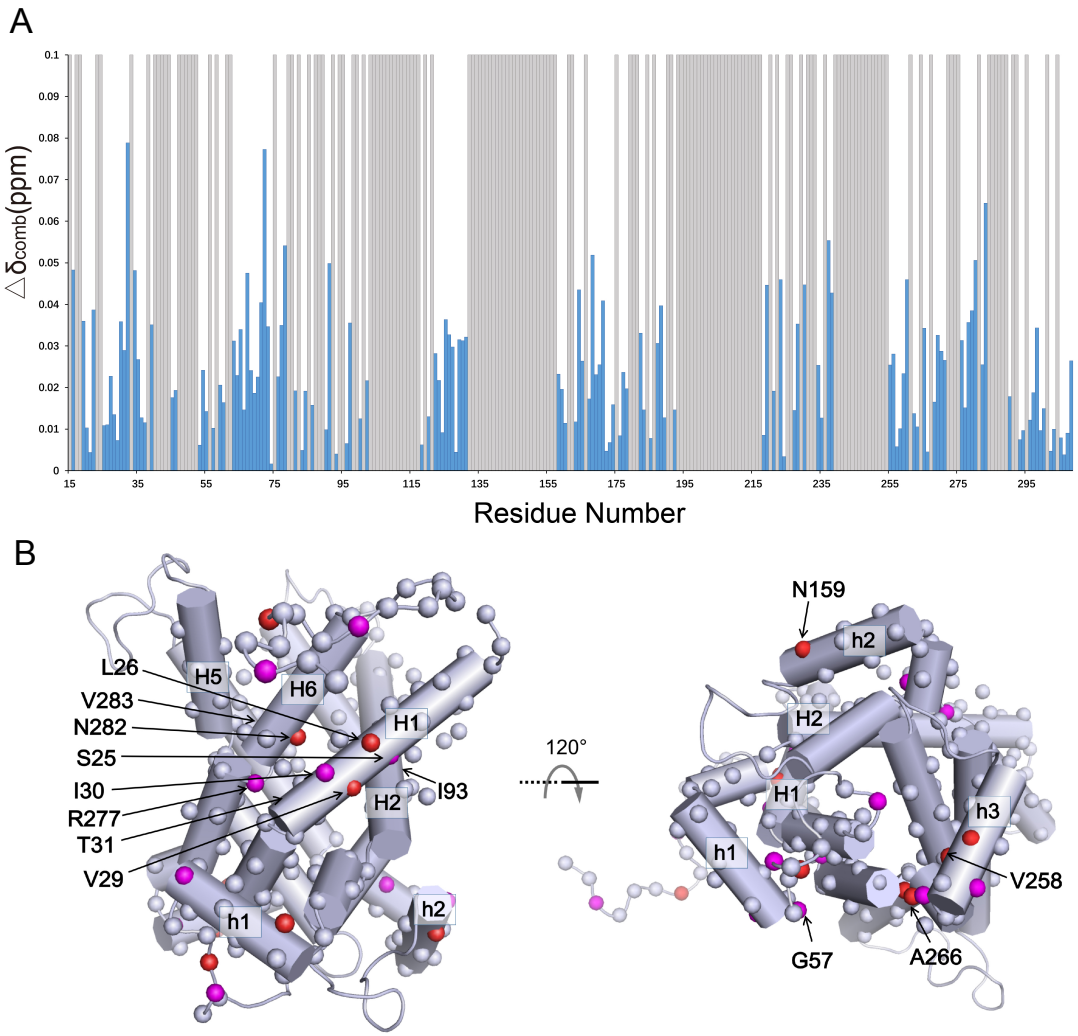

Figure S2. Chemical shift perturbation of UCP1 induced by C16FA, Related to Figure 3C.

(A) Residue-specific chemical shift changes caused by C16FA (10 mM). The grey bars indicate residues for which measurement could not be performed due to missing assignment or resonance overlap.

(B) Mapping the residues with higher apparent C16FA affinities onto the UCP1 model based on AAC crystal structure (PDB code: 1OKC). Spheres represent analyzed residues. Red spheres represent residues with $K_D \leq 700$ μM, magenta sphere represent 700 μM < K_D <1200 μM. White sphere represent $K_D \geq 1200$ μM.

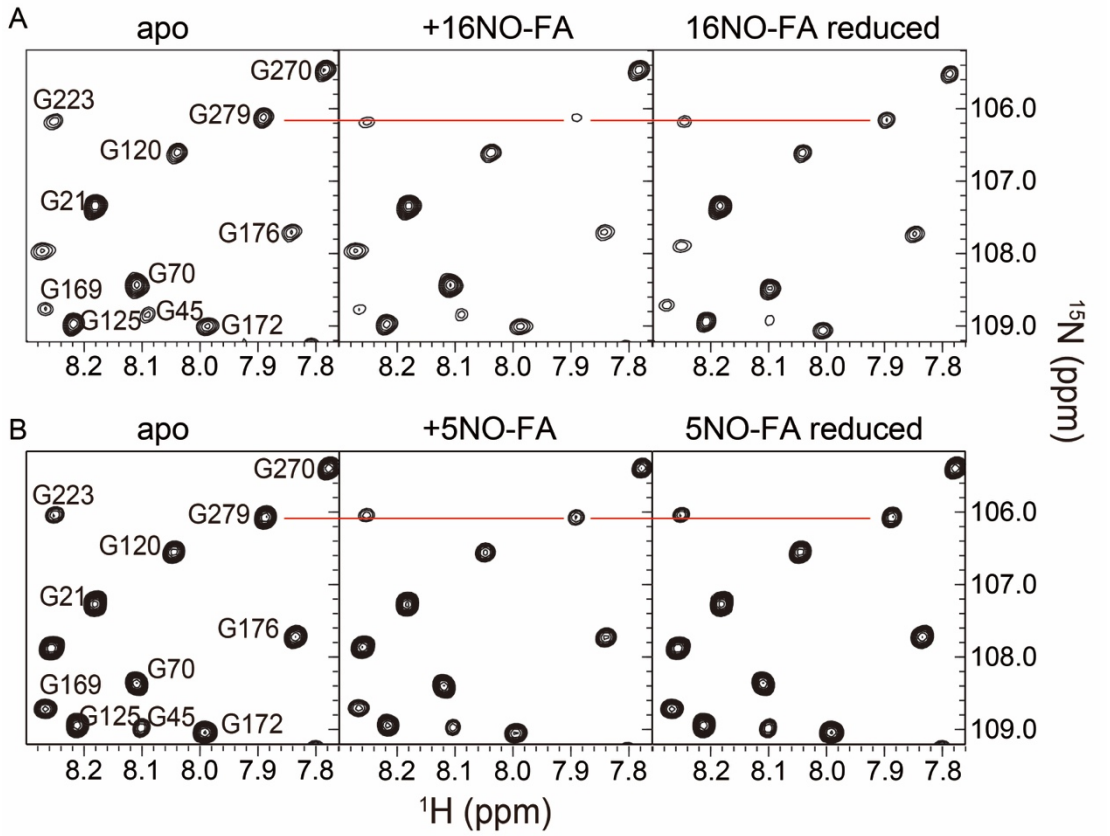

Figure S3. Related to Figure 4.
G279 shows specific broadening by nitroxide-labeled FAs (16NO-FA, A; 5NO-FA, B) and the recovery of broadened peaks by the addition of ascorbic acid.

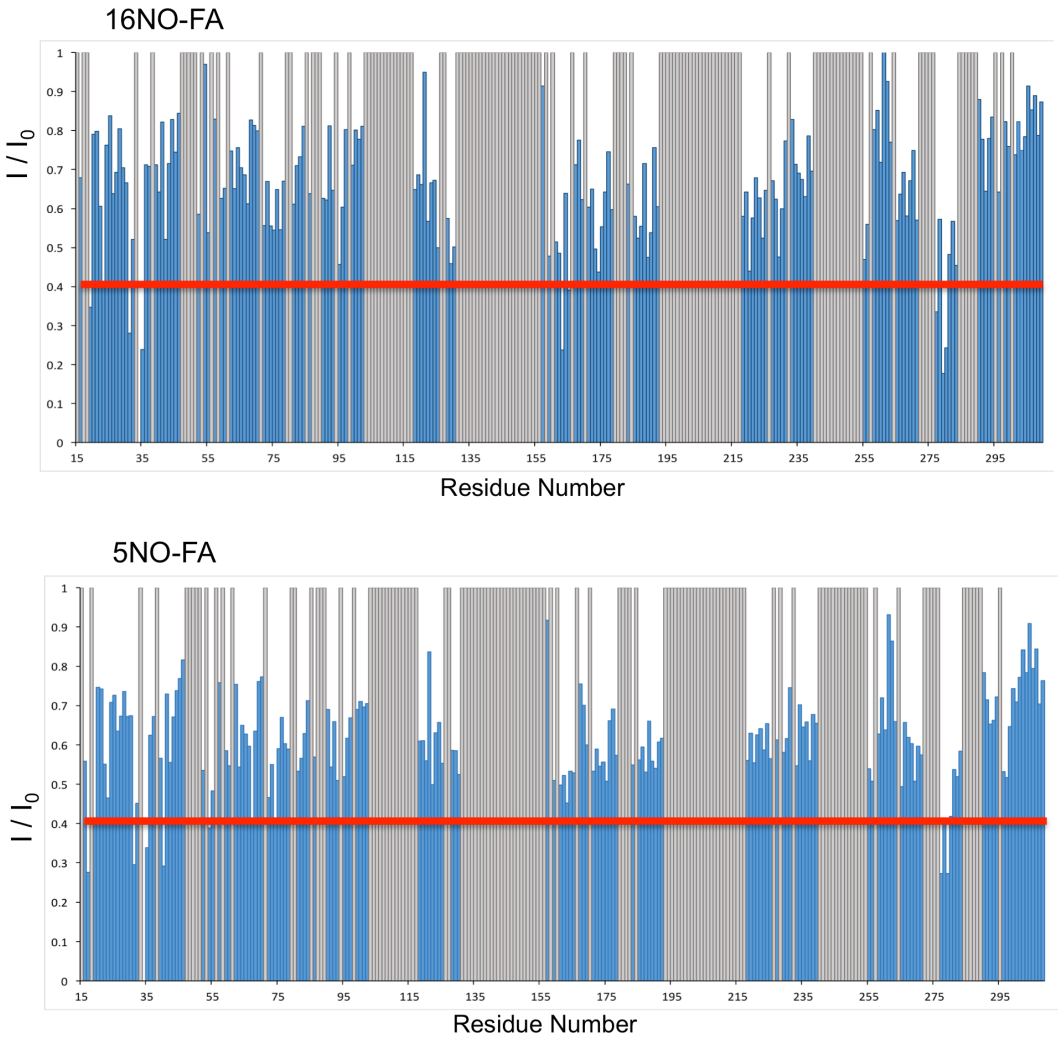

Figure S4. Related to Figure 4.

Residue-specific I/I_0, where I and I_0 represent the peak intensity measured in the presence and absence of spin-labeled FA, respectively. The grey bars indicate residues for which PRE measurement could not be performed due to lack of assignment or resonance overlap. The I/I_0 cutoff of 0.4 was chosen to highlight residues with I/I_0 values that are below the I/I_0 fluctuation across the plot.

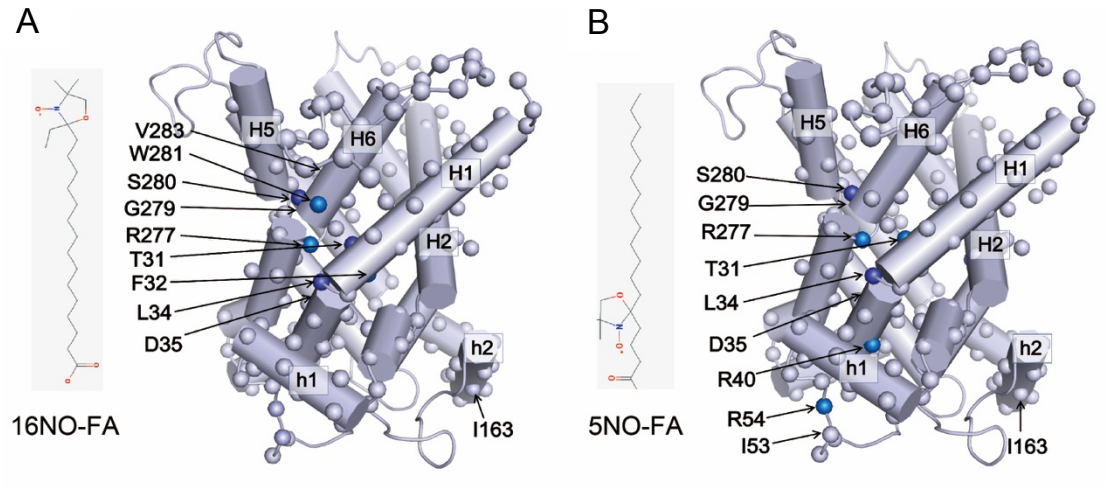

Figure S5. Related to Figure 4.

Mapping of the PRE effects under 16NO-FA (A) and 5NO-FA (B) onto the UCP1 model based on AAC crystal structure (PDB code: 1OKC). Spheres represent assigned backbone amide. Blue spheres represent residues which I/I_0 ratio < 0.4.

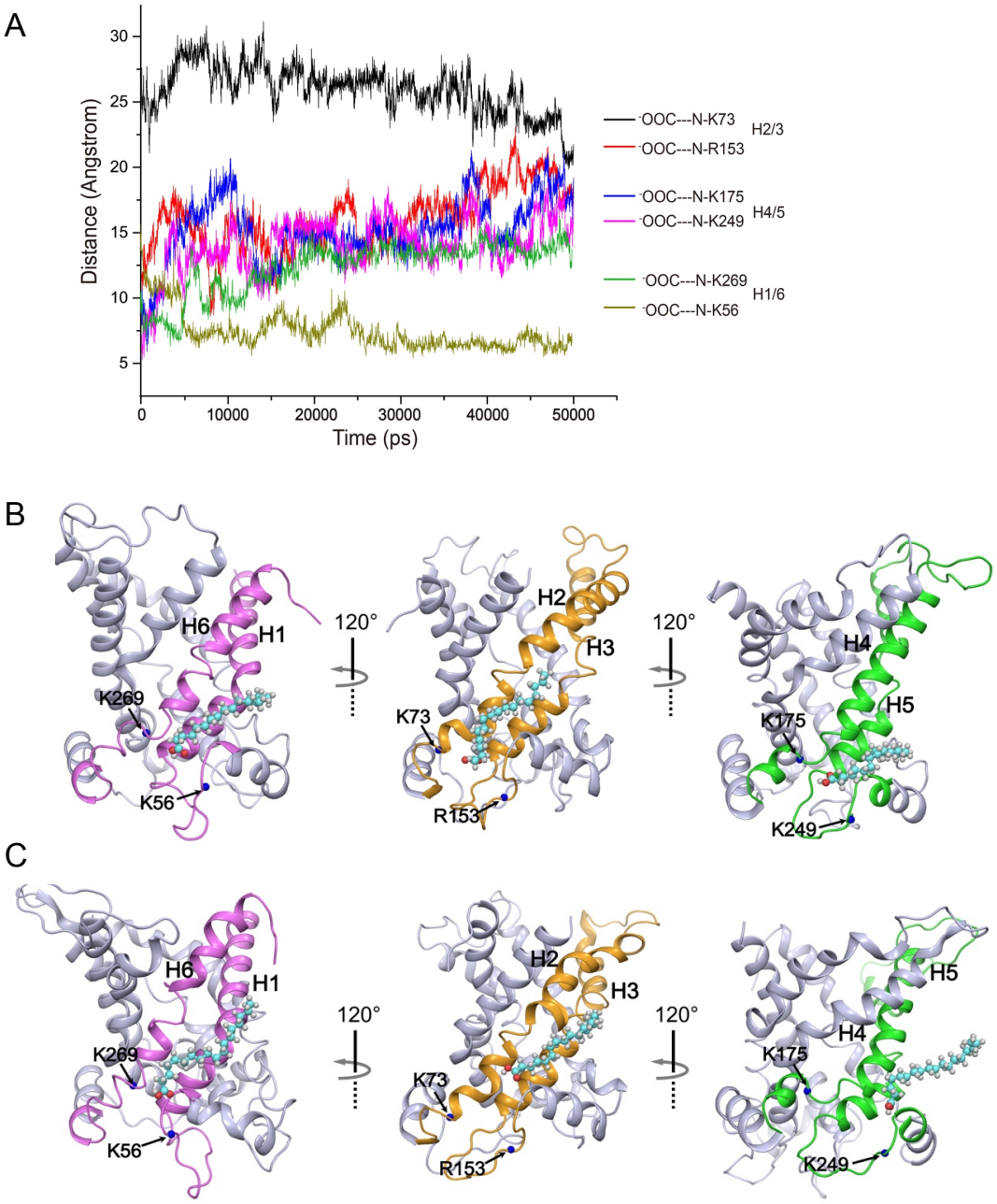

Figure S6. Related to Figure 5.

(A) The monitored distances between the UCP1 backbone amide nitrogen atoms of residues indicated by blue balls in Fig. 5B and the carbon atoms of the carboxyl groups of C16FA. The time scales indicate that the conformations of C16FA-UCP1 complex was dynamic during the MD simulation.

(B) Stability of C16FA binding to UCP1 model based on AAC crystal structure (PDB code: 1OKC) in MD simulation. The initial positions of C16FAs at three helix-helix interface sites that afford charge-charge interactions with the FA carboxylate head group. These sites include the PRE-derived site at the H1-H6 interface (pink), the K73/R153 site at H2-H3 interface (orange), and the K175/K249 site at the H4-H5 interface (green).

(B) The average positions of C16FAs after 50 ns MD simulation.